

Research Paper

Quantitative Analysis of Eukaryotic Protist Cells Using Image Processing with Epson Perfection V750 Pro & MATLAB

Yuzo Iano¹, Daniel Katz Bonello^{2*}, Umberto Bonello Neto³

^{1,2,3}Department of Communications/ School of Electrical and Computer Engineering (FEEC), University of Campinas, Campinas, Brazil

*Corresponding Author: daniel.bonello91@gmail.com

Received: 22/Apr/2023; Accepted: 25/May/2023; Published: 30/Jun/2023

Abstract— Biomedical engineering is the link between engineering health sciences, and society. In this way, the biomedical engineer works in the development maintenance and assembly of equipment and programs to carry out diagnoses and treatments carried out by health professionals, such as: physicians, biomedical engineers, and dentists. In addition, can also manage the area of equipment purchases and develop scientific research on biomedical materials and instruments. Among the places where this professional works are: hospitals, medical clinics, health centers, pharmaceutical and clinical analysis laboratories, companies specialized in hospital maintenance and research centers. Therefore, the aim of this article is to propose a quantitative analysis of eukaryotic protist cells using image processing with a microscopy – Epson Perfection V750 and MATLAB-R2020 image analysis code. Thus, as results, were obtained a dataset of 14 eukaryotic detected cells samples using the MATLAB-R2020, and then a measurement pattern was utilized to quantify these 14 patterns, according the following premises: the sample number (from “sample 1” to “sample 14”); number of detected circles in eukaryotic cells images; sensitivity position of detection; edge threshold position; utilized method (phase code); object polarity (bright); and radius range (from 10 μ m to 30 μ m). As final results, the maximum numbers of detected circles were 287, and the minimum number of detected circles was 1 detection: utilizing a threshold of 0.3. Now utilizing a threshold form 0.2 to 0.94 (percentage difference of 370%), the maximum number of detected circles were 218 elements and the minimum number of detected circles were 7 elements (percentage difference about 3,000%). In conclusion, this experiment has obtained a better detection of circular elements in eukaryotic protist cells when the sensitivity position is seted at 0.99 and the edge threshold position is about 0.3: within phase code method, bright object polarity and radius range between 10 μ m and 30 μ m. These values were obtained using MATLAB-R2020.

Keywords— Eukaryotic cells, MATLAB, image processing, pattern recognition, quantitative analysis, spectrometry.

1. Introduction

Pharmaceutical and biotechnology companies (biopharmaceutical) continue to benefit from solid drug development pipelines, while development advances in the industry as a whole has seen increased support for the return of demand for elective procedures: drug sales, medical sales of drugs, medical equipment, and equipment, as the overall impacts of the pandemic on hospital utilization has been decreasing. By most measures, the valuations of the sector have been relatively attractive until 2022 [1]. The **Figure 1** represents the annual FDA drugs approval. Thus, it's possible to identify that from 2015 to 2021, was developed more than 48 new drugs per year. Hence, 50 drugs have been approved in 2021.

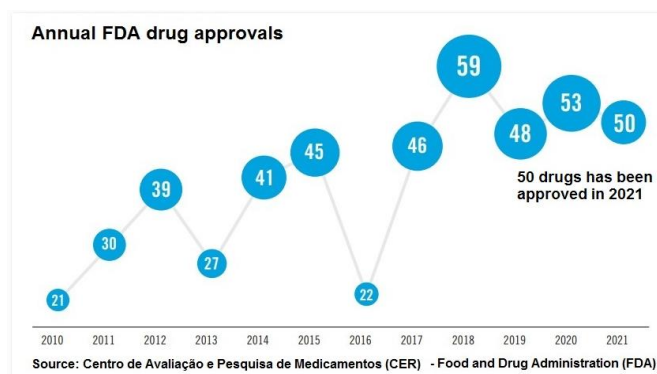


Figure 1. Annual FDA drug approvals

Therefore, concurrently, there is a surge of novel drug discovery and biotech companies that are established as AI-centric organizations [2]. In addition, there is a growing in global demand for drug discovery [3].

In that case, increasing in the use of advanced technologies and identifying the best drug discovery candidates. Therefore,

the diagnosis of important diseases is based on a robust growth of medical exams and clinical devices. Still, the gradual increase in health spending regionally assists the new advances in resources of drug discovery [4].

Above all, the aim of this article is to propose a quantitative analysis of eukaryotic protist cells using image processing with a microscopy – Epson Perfection V750 and MATLAB-R2020 image analysis code. Thus, as results, were obtained a dataset of 14 eukaryotic detected cells samples using the MATLAB-R2020, and then a measurement pattern was utilized to quantify these 14 patterns, according the following premises: the sample number (from “sample 1” to “sample 14”); number of detected circles in eukaryotic cells images; sensitivity position of detection; edge threshold position; utilized method (phase code); object polarity (bright); and radius range (from 10µm to 30µm).

As final results, the maximum numbers of detected circles were 287, and the minimum number of detected circles was 1 detection: utilizing a threshold of 0.3. Now utilizing a threshold form 0.2 to 0.94 (percentage difference of 370%), the maximum number of detected circles were 218 elements and the minimum number of detected circles were 7 elements (percentage difference about 3,000%). In conclusion, this experiment has obtained a better detection of circular elements in eukaryotic protist cells when the sensitivity position is setted at 0.99 and the edge threshold position is about 0.3: within phase code method, bright object polarity and radius range between 10µm and 30µm. These values were obtained using MATLAB-R2020.

2. Related Work

The proposed work in [5] shows that cancer cancer cells diseases can be predicted using a coupled circuit. Thus, as results, were obtained an endomembrane monomeric (Arf1) and heterotrimeric (Gi) GTPase coupled circuit, as shown the following **Figure 2**. The **Figure 2** represents the GTPase coupled circuit, where in the first stage named “A” is located the endomembrane, after occurs the chemical and biological reactions the frame 2, while in the frame 3 it’s possible to observe that GTPase is growing from the given linker in two different environments, for example.

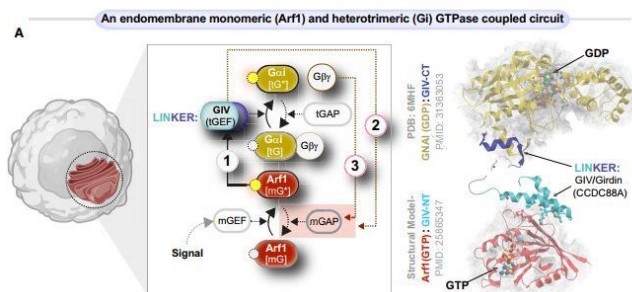


Figure 2. Endomembrane monomeric (Arf1) and heterotrimeric (Gi) GTPase coupled circuit

Now in [6] was proposed a new potential drug discovery researched method based on brazilian biodiversity. The

Figure 3 shows an example of chemical bonding of monoalid drug and your teutomeric structures. In the **Figure 3** is also possible to observe that carbon structure of monoalid (43) has a chemical reaction with hydroxyl-aldehyde form of the monoalide. Hence, that chemical carbon chain element reacts with aldehyde-acid form of the monoalide, becoming into an open form of monoalide.

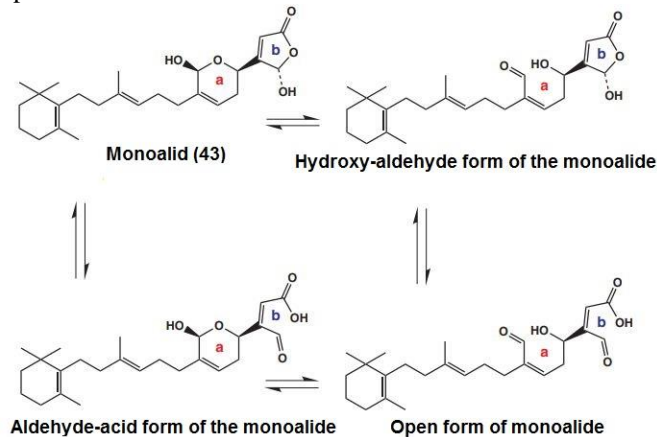


Figure 3. Monoalid drug and your teutomeric structures

In the work [7] regarding to the usage of artificial intelligence (AI) for streamlined classification of microscopic blood cell images, was proposed a transfer-learning model. This **Figure 4** represents the state of the art from a transfer-learning model to learning stands. Explaining the blocks in this figure, first of all, a dataset is inputted in the architecture. Thus, a pre-trained supervision algorithm model supplies the construction of a head model, which redirects this information to a transfer learning. As a final step, the program is able to make a dataset classification based on pre-trained selected models.

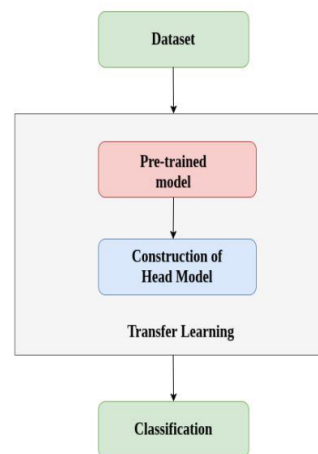


Figure 4. A transfer-learning model to learning stands

Still regarding to the blood cells investigation analysis and classification, the work proposed in [8] studies blood cells. Thus, as obtained results the **Figure 5** indicates two samples of detected elements. In the **Figure 5**, it’s possible to observe the gray-scale about the microscopic images of immunobeads. The radius for detected elements was configured in 50µm, and it’s possible to observe that in the image (a) there are more canonical elements and bright circles formed in this sample. Now in the image (b) there are some bright circular elements in this taken sample.

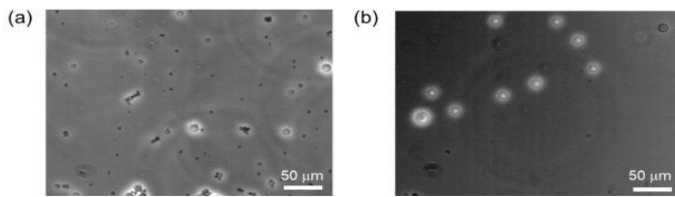


Figure 5. Microscopic images of immunobeads

Now looking in the work [9] it's possible the implementing algorithm in C++ builder. Still, in the **Figure 6** it's possible to observe the various stages of a brain scanned elements. Therefore, in the stage (1) shows a brain without the bright contrast implemented by the C++ algorithm. Now in the stage (2), (3) and (4) it's possible to observe that lesions are detected in a brain using artificial immune systems (AIS) and a support vector machines (SVM). Finally in the stage (5) it's possible to observe more bright detected multiple sclerosis (MS).

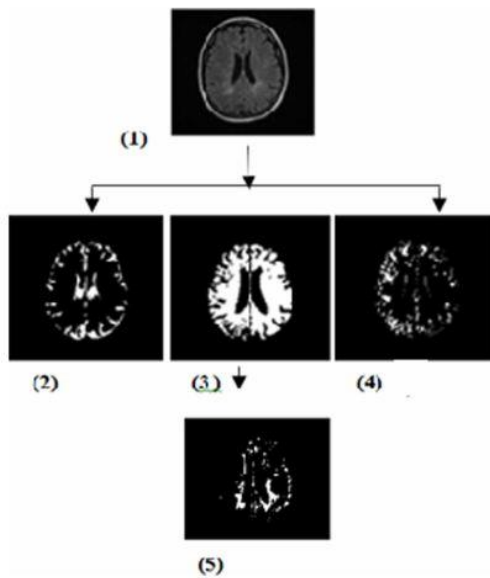


Figure 6. MS lesions detected by SVM

Regarding to the work [10] the authors were focused in image processing techniques. In addition, the results of this research shown in the **Figure 7**, that it's possible to observe that in the first stage of the proposed AI architecture. There are important learning elements, such as: perceptron; recurrent neural network; feed/forward network; boltzman network; convolutional neural network. Therefore, these learning elements are linked into the artificial neural network (Neural Net), which is an interface between machine learning (ML) and those entry learning elements. Furthermore, in the middle of this block, it's possible to observe the Artificial Intelligence (AI), element that makes supervision over Machine Learning and Decision Tree (Non-Parametric Supervised) algorithm, which are divided into Random Forest and Classification & Regression Tree. Finally in the right side of the block chain flowchart, it's presented the elements which makes interface with the Instance-Based (Memory-Based) Algorithm, they are: Support Vector Machine; K-Nearest Neighbour; and Self Organized Map, for example.

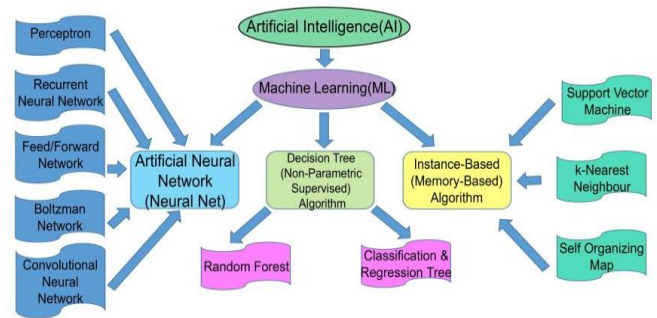


Figure 7. Summarized notion of AI and ML tools engaged in drug discovery and development

In work [11] was studied a method appointed in **Figure 8**, that shows DESI-MSI images of horizontal 10µm thick section in deep dermis and the transition to the subcutaneous tissue, for example. Also in the **Figure 8** it's possible to observe that in the upper spectrum, there are different values of thickness in the deep dermis, such as: 1010µm, 1250µm, 1620µm and 1870µm. Now, in the down frame these elements have been shown to make a transition to the subcutaneous tissue. Indicating that it's possible to discover novel therapies from the drug permeated cell membranes.

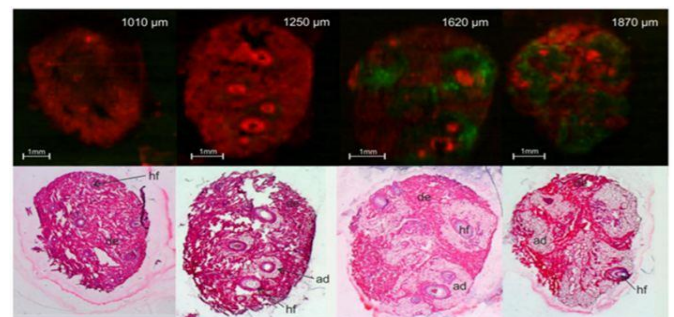


Figure 8. DESI-MSI images of horizontal 10µm thick section in deep dermis and the transition to the subcutaneous tissue

Now in work [12] authors treats the COVID-19 issue as a research regarding to the COVID-19 The **Figure 9** are presented a Sars Cov-2 detection architecture that shows, in the first frame, the input CT image of a cell. Hence, the algorithm runs using an adjacency matrix in the frame 2. There is a graph feature extraction in the frame 3, turning into a graph convolution on frame 4. After algorithm analyzes the pattern obtained data, there are two possible classifications using the analyzed image: non-Covid-19 and positive test to Covid-19.

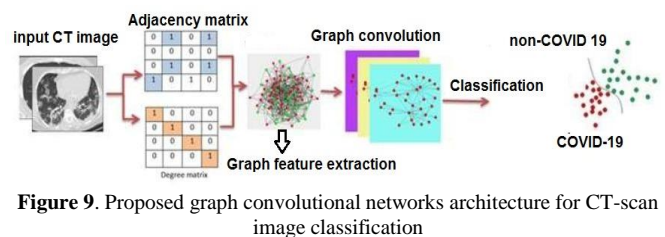


Figure 9. Proposed graph convolutional networks architecture for CT-scan image classification

Furthermore, in the work [13] authors established a method in the **Figure 10** that shows the proposed artificial intelligence architecture for Covid-19 detection and diagnosis: in the first frame, are proposed a supervised system, machine learning

algorithm and a final unsupervised system. Now in the second frame, it's possible to observe an AI models for Covid-19 detection, which makes some interface between the elements of the first frame and third frame. Finally in the third frame its possible note that there are elements such as: object detection; image segmentation; deep learning; transfer learning; and shot learning.

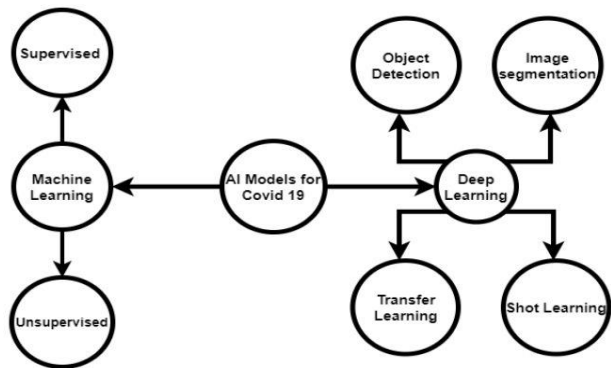


Figure 10. Overview of AI approaches for COVID-19

Finally, in research [14] authors uses multivariate method appointed in the Figure 11. It's possible to observe two images: the compound 1, showing the ligand-receptor complexes and the compound 2, indicating the pixels of molecules structures. Thus, these models were obtained in 2D and 3D forms, which are represented below. Furthermore, was utilized some techniques, such as: multivariate calibration, multiple linear regression, component regression, partial last squares regression, and genetic algorithms.

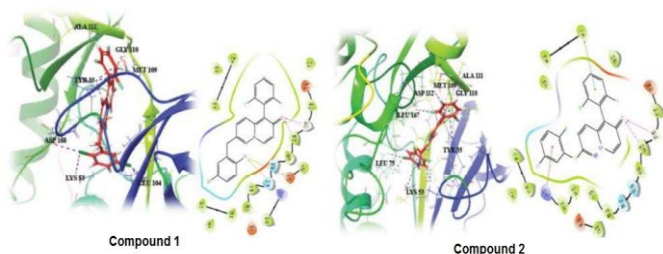


Figure 11. The 2D and 3D images of ligand-receptor complexes related to highlighted poses

3. Comparing prokaryotic and eukaryotic cells

The following three figures show schematic representations of a prokaryotic cell and two eukaryotic cells, one exemplifying an animal cell and the other, a plant cell. These schematics were made based on observations under the electron microscope. In this way, the structures of the cytoplasm are compared and the origin and evolution of the cells can be identified [15]. In the Figure 12 it's possible to observe a schematic of animal (eukaryotic) cell with part of the cell removed. Thus, it measures about 20µm in diameter and also is possible to observe the following elements, for example: mitochondria; core (composed by karyotheca, chromatin and nucleolus); granular endoplasmic reticulum (rough); plasmatic membrane; non-granular (smooth) endoplasmic reticulum; golsiense complex; microtubules; ribosomes; centrioles; peroxisome and microfilaments.

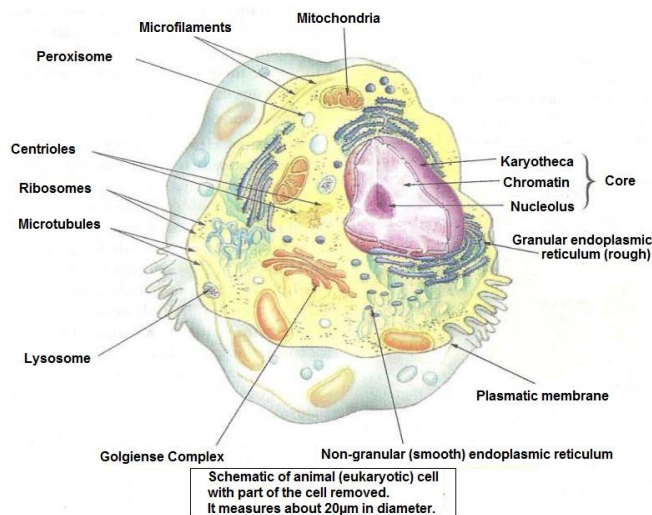


Figure 12. Schematic of a eukaryotic animal cell

The cytoplasm of the prokaryotic cell is much simpler than that of the eukaryotic cell, even when analyzed under the electron microscope. It consists of a matrix rich in water, with various ions and molecules dissolved in it. Therefore, it is a cytoplasm in which there are no membrane-bound structures. Exceptions to this generalization are described in the Figure 13, which represents a schematic of a eukaryotic plant cell, composed by the following elements: mitochondria; chloroplast; vacuole; ribosomes; plasmodesms; golgiense complex; plasmatic membrane; cell wall; non-granular (smooth) endoplasmic reticulum; granular (rough) endoplasmic reticulum; and core.

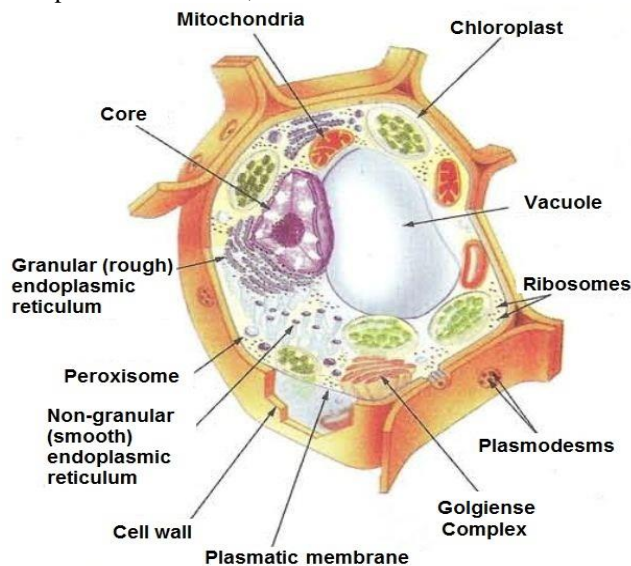


Figure 13. Schematic of a eukaryotic plant cell

- **The mesosome** - invagination of the plasma membrane into the cytoplasm; it is present in some types of bacteria;
- **The photosynthetic membranes** - are present in the cytoplasm of cyanobacteria; chlorophyll molecules are located in these membranes, which are therefore related to photosynthesis.

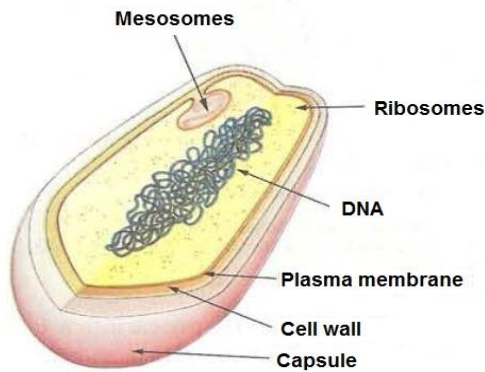


Figure 14. Schematic of a bacteria cell

In addition, immersed in the cytoplasm of prokaryotic cells are ribosomes - small grain-like structures without a delimiting membrane. They are made up of proteins associated with a type of nucleic acid called ribosomal ribonucleic acid (rRNA). In other words, ribosomes are concerned with protein synthesis and occur in eukaryotic cells as well [15]. Represented in the **Figure 14**, the schematic of a bacteria cell is composed by the following elements: mesosomes; ribosomes; DNA; plasma membrane; cell wall; and capsule.

In the cytoplasmic matrix of prokaryotic cells the genetic material is dispersed, consisting of a single circular DNA molecule. This region of the cell is called the nucleoid. There is no membrane separating the nucleoid from the rest of the cytoplasm. In summary, in eukaryotic cells, the genetic material is separated from the cytoplasm by a membranous structure called the karyotheca, forming the nucleus. In prokaryotic cells there is thus no nucleus [15].

In addition to the DNA located in the nucleoid, in the cytoplasm of prokaryotic cells there may be one or several small circular DNA molecules called plasmids, which contain genes generally related to the resistance of bacteria to antibiotics. The cytoplasm of eukaryotic cells, on the other hand, corresponds to the entire region situated between the plasma membrane and the carioteca. It consists of a fluid called cytosol (or cytosol, or hyaloplasm, or even fundamental cytoplasm), composed basically of water, ions, and substances necessary for the synthesis of organic molecules, in which the following structures are immersed:

- **Ribosomes;**
- **Cytoplasmic inclusions** - Temporary, non-membranous structures that generally represent forms of reserve of substances in the cell. Glycogen molecules, for example, can be stored in the cytosol of animal cells or in that of fungi, in microgranules, to which enzymes adhere, performing glycogen synthesis or degradation, according to the cell's needs. Another example is fat, which accumulates in animal cells forming drops that, in adipose cells, can occupy almost the entire cytosol. These fat drops are fatty acid reserves;
- **Cytoskeleton** - Responsible for the shape and internal support of the cell, for the movement of the cytoplasm, and for the concentration of muscle cells;

- **Membranous organelles** - Membrane-bound structures. The membranous organelles present in virtually all eukaryotic cells are: endoplasmic reticulum, golgiense complex (Golgi apparatus and complex), lysosomes, peroxisomes, and mitochondria. Chloroplasts occur only in cells of photosynthesizing eukaryotic organisms, and cell juice vacuoles occur in the cells of multicellular plants and algae.

Membranous organelles represent about 40% of the total volume of a cell. This is, however, an average value and varies from cell to cell in the same individual, from species to species, and from kingdom to kingdom. Moreover, this percentage also depends on the metabolic activity of the cell [15].

4. Light Microscopes

The study of smaller structures is done with light microscopes, which allow magnifications of up to 1,500 times. At these magnifications, however, it is not possible to see the details of cell structure [15].

Light Microscope

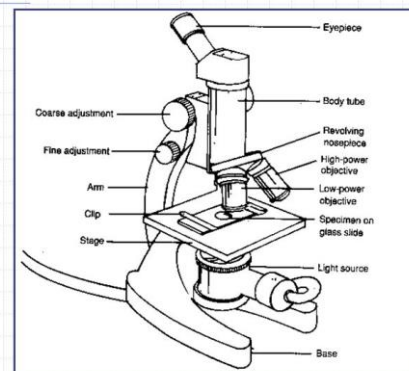


Figure 15. Light microscope

The microscope shown in **Figure 15** is called a stereoscope (commonly known as a magnifying glass). It is suitable for observing structures and organisms larger than those normally observed in microscopes as shown in **Figure 16**, and also allow the observation of opaque objects. The microscope shown in **Figure 16** allows higher magnifications than stereoscopic microscopes, and the objects to be analyzed must allow light to pass through. The magnification of the image we see in the compound microscope is given by multiplying the magnification of the eyepiece by the magnification of the objective. For example, a compound microscope with a 5X eyepiece and 40X objective provides 200X magnification.

5. Electronic Microscopes

Detailed study of cell structures has only been possible with the advent of electron microscopes (EM), which allow cells to be observed at much higher magnifications. This is possible because electron microscopes use electron beams to analyze the object to be studied, instead of light beams [15].

Electron microscopes can be either transmission or scanning. Transmission electron microscopes are used to analyze structures cut into very thin slices. Scanning microscopes are used to analyze the surface of the body of living things, of cells, and even of molecules.

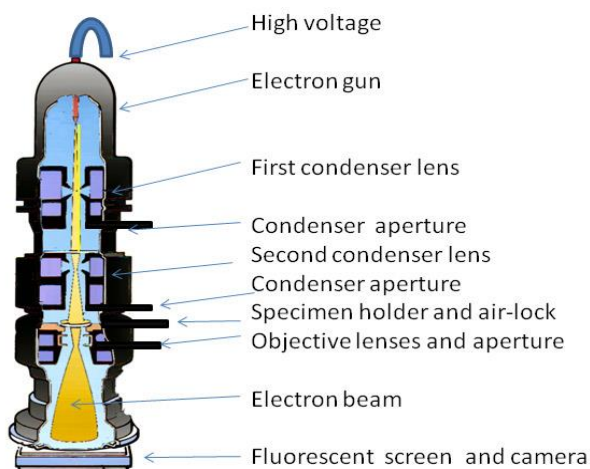


Figure 16. Electronic microscope

The material to be analyzed in the (EM) should be properly fixed and stained with heavy-matter salts that provide contrast in the structures of the cells. These stains make the cell structures less permeable to electron beams, so that the most stained structures are seen in black or dark gray and the least stained structures are seen in light gray tones.

The image is viewed on a screen and can be printed as a photograph. Because they are always black and white, these photos can later be artificially colored in an effort to bring out the cellular structures even more. In this way, photos taken with the use of different types of microscopes are called photomicrographs or simply micrographs [15].

6. The Epson Perfection V750 Pro Microscope & MATLAB R2020 software

The following **Table 1** represents the general characteristics of Epson Perfection V750 Pro Microscope. While **Table 2** shows the electrical characteristics, and **Table 3** appoints to the mechanical characteristics in concern to this device. Finally, in the **Table 4** are described the interfaces that Epson Perfection V750 Pro Microscope demands. In the **Table 1**, there are 2 columns and 10 lines: in the first column, are represented: the microscope type; utilized photoelectric device; effective pixels; document size; image resolution; output resolution; image data; interface; and light source. While in the second column, there are the respective general characteristics of Epson Perfection V750 Pro Microscope.

Table 1. General characteristics of Epson Perfection V750 Pro Microscope

Microscope type	Desk color microscope
Photoelectric device	Color CCD line sensor
Effective pixels	40800 × 56160 pixels at 4800 dpi The scanning area may be restricted if the resolution setting is large.
Document size	Reflective: 216 × 297 mm (8.5 × 11.7 inches) A4 or US letter format

Document size	Transparent: 203.2 × 254 mm (8 × 10 inches) (Four strips of 35mm film [6 frames each], twelve 35mm slides, two frames of 6 × 20 cm (6 × 20 cm) medium format film, or two frames of 4 × 5 inch (4 × 5 inch) film)
Image resolution	4800 dpi (main scan: 6-line CCD optical resolution of 122,400 pixels)
Output resolution	6400 dpi (main scan: 6-line CCD optical resolution with 113,280 pixels)
Image Data	9600 dpi with Micro Step 25 to 12,800 ppi (1 ppi steps)
Interface	Internal: 16 bits/pixel/color External: 16 bits/pixel/color (max)
Light source	One high-speed USB port Cold-cathode fluorescent lamp, white, infrared LED

The **Table 2** represents the electrical characteristics of Epson Perfection V750 Pro Microscope. This table is composed by 2 columns and 3 lines: in the first column, are represented: the rated voltage; input current; and consumption, respectively. While in the second column, there are the respective electrical characteristics of Epson Perfection V750 Microscope.

Table 2. Electrical characteristics of Epson Perfection V750 Pro Microscope

Rated voltage	DC 24 V
Input current	1,3 A 32 W in operation
Consumption	21 W in ready mode 4 W in sleep mode 0.5 W off

The **Table 3** represents the mechanical characteristics of Epson Perfection V750 Pro Microscope. This table is composed by 2 columns and 2 lines: in the first column, are represented: dimensions; and the weight of this device, respectively. While in the second column, there are the respective mechanical characteristics of Epson Perfection V750 Microscope.

Table 3. Mechanical characteristics of Epson Perfection V750 Pro Microscope

Dimensions	Width: 503 mm (19.8 inches) Depth: 308 mm (12.1 inches) Height: 152,5 mm (6,0 inches)
Weight	Approx. 6.6 kg (14.5 lb)

The **Table 4** represents interfaces of Epson Perfection V750 Pro Microscope. This table is composed by 2 columns and 3 lines: in the first column, are represented: the interface type; electrical standard; and connector type, respectively. While in the second column, there are the respective interfaces characteristics of Epson Perfection V750 Microscope.

Table 4. Interfaces of Epson Perfection V750 Pro Microscope

Interface Type	Revision 2.0 of the Universal Serial Bus Specifications Full-speed mode (12 Mbits/second) and high-speed mode (480 Mbits/second) of the Universal Serial Bus revision 2.0 standard.
Electrical Standard	One door (type B)
Connector Type	

Now the following **Table 5** shows the settings concepts of MATLAB R2020 path installation. This table is composed by 2 columns and 9 lines: in the first columns, are represented: the language fundamentals of MATLAB R-2020; data import and analysis; mathematics characteristics; graphics concepts; programming features; app building; software development tools; external language interfaces; environment and setting, respectively. While in the second column, there are the respective characteristics of software MATLAB R-2020, for example.

Table 5. Setting concepts of MATLAB R2020 path installation

Column1	Column2
Language Fundamentals	Syntax, array indexing and manipulation, data types, operators
Data Import and Analysis	Import and export data, including large files; preprocess data, visualize and explore
Mathematics	Linear algebra, differentiation and integrals, Fourier transforms, and other mathematics
Graphics	Two- and three-dimensional plots, images, animation
Programming	Scripts, functions, and classes
App Building	Create self-contained apps, embedded Live Editor tasks, and custom UI components
Software Development Tools	Debugging and testing, organizing large projects, source control integration, toolbox packaging
External Language Interfaces	External language and library interfaces, including Python, Java, C, C++, .NET, and Web services
Environment and Settings	Preferences and settings, platform differences, adding hardware and optional features

7. Theory/Calculation

There is a work in [16] that proposes a theoretical calculation. This presented theory in this section is a practical development from image processing formulas and concepts which can be utilized in the experimental method in this current work, for example. Furthermore, check above the mathematic modeling of an image inspection system using the Microscope Epson Perfection V750 and MATLAB R2020 as elements of image circle detection in eukaryotic protest cells:

The eukaryotic image processing technique is presented in the Eq.(1):

$$T = T[x, y, p(x,y), f(x,y)] \tag{1}$$

The threshold relation is presented in the Eq.(2):

$$g(x,y) = \begin{cases} 1 & \text{if } f(x,y) > T \\ 0 & \text{if } f(x,y) \leq T \end{cases} \tag{2}$$

Now in concern to the eukaryotic protist cells, was possible to producing samples and circular associations on digital layouts. The **Figure 17** shows an example of eukaryotic cell sample taken from the Microscope Epson Perfection V750:

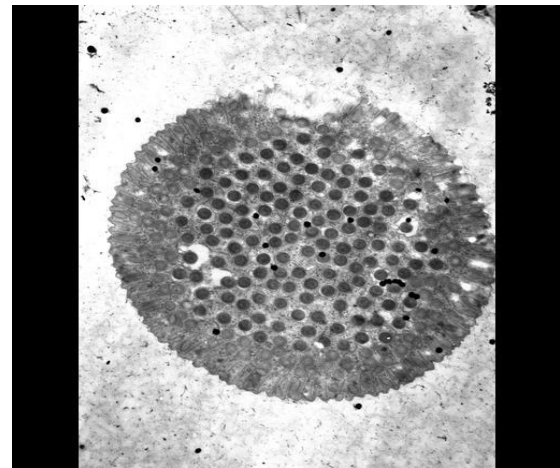


Figure 17. Example of eukaryotic protist cell taken from the Microscope Epson Perfection V750

Thus, to detect circular elements in eukaryotic protist cells, as shown the Figure 17, its necessary, firstly, apply the Hough Transform as a procedure in computer vision used in straight line and curves [17]. The Hough Transform also was utilized [18]. There are some works [19] that describes the Eq.(3):

$$(x - a)^2 + (y - b)^2 = r^2 \tag{3}$$

Therefore, the quantity is delimited by the coordinate (x, y) that can generate a circle in (a – b) space parameter.

8. Experimental Method/Procedure/Design

About the algorithm used in eukaryotic cells detection, the script is represented bellow for this current proposed work. Furthermore, was developed a flowchart of this script, represented in the **Figure 18** of this section.

In concern to the steps of the adopted methodology, a circle detection algorithm was developed in MATLAB R-2020, using the concepts of the Hough Transform and the general equation for the detection of circles in images, for example. Therefore, as we can see in the realized architecture, first the image of the original eukaryotic cell is inserted into the MATLAB graphical interface. Next, pre-processing of the image occurs with binarization and application of threshold between 0.3 and 0.94.

Consequently, the next step in this flow consists of detecting circular elements of the image through the concept of edge detection. Therefore, as a semifinal step in the algorithm logic, the program must now apply the Hough Transform in line or circular detection, where in this case, this transform will be responsible for detecting circles in the eukaryotic cells inserted with the algorithm.

At the end of all image processing steps, the result of the circular detection is marked with a line in the final image. Thus, the experimental method for this algorithm is composed of the steps in the flowchart in Figure 18 and the experimental design is represented by the lines of code of the algorithm developed in MATLAB R-2020.

• **Algorithm for eukaryotic cells circle detection in MATLAB R 2020:**

```

classdef CircleFinderApp < handle
%
% Usage:
% app.CircleFinderApp

properties
AppHandle;

CircleFinderApp.refcount(obj.Increment);

% Verify we are about to execute the correct function - if not we
% should error and exit now. We need to make sure the paths are
% equal using canonical paths.
existVal = exist(fullfile(pwd,'circleFinder')); % #ok<EXIST>
doesShadowExist = existVal >= 2 && existVal <= 6;

pathOne = java.io.File(pwd);
pathOne = pathOne.getCanonicalPath();
pathTwo = java.io.File(obj.AppPath{1});
pathTwo = pathTwo.getCanonicalPath();

if (doesShadowExist && ~pathOne.equals(pathTwo))
% We are trying to execute the wrong circleFinder
errorDlg(message('MATLAB:apps:runapp:WrongEntryPoint',
'circleFinder').getString, ...
message('MATLAB:apps:runapp:WrongEntryPointTitle').getString);
appinstall.internal.stopapp([],[],obj)
return;
end
    
```

• **Flowchart for the developed script in MATLAB R 2020:**

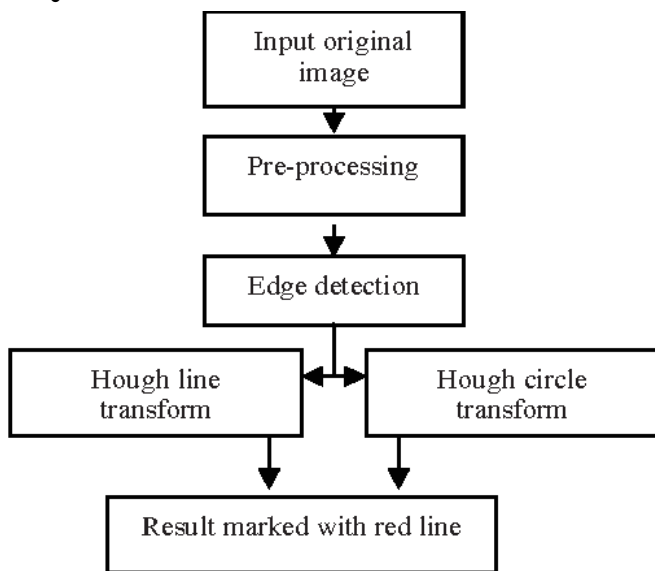


Figure 18. Flowchart for eukaryotic cells circle detection

9. Results and Discussion

First of all, as results were obtained 14 eukaryotic detected cells samples using the script developed using MATLAB R2020 presented in the previous section. Therefore, a measurement pattern was utilized to quantify these 14 patterns, according to the following premises below.

Therefore, regarding the results, four graphs were obtained: the first, showing the number of circles detected according to the sample; the second graph showing the number of circles detected according to the sensitivity position; the third graph, indicating the number of circles detected by the threshold edge position; and the fourth graph, pointing to the percentage difference between the parameters adopted in the algorithm, i.e. number of circles detected, edge threshold position and sensitivity position.

- **The sample number (from “sample 1” to “sample 14”):** those samples were obtained from a dataset base, which the same eukaryotic protist cell was inputted in the MATLAB algorithm, generating 14 sampling results with different number of detected circles;
- **Number of detected circles in eukaryotic cells images:** as results appoints, the maximum number of detected circles were 287 elements, in the 5th sample. While the lowest number of detected circles was about 1 element, in the 1st sample. Furthermore, the standard deviation (σ) for detected circles in the developed algorithm, has as value equals to $\sigma = 86.19$;
- **Sensitivity position of detection:** as results appoints, the maximum value of sensitivity position were 0.98 or magnified x 100 equals to 98, keeping this constant value from the 4th sample to the 14th sample. While the lowest value of sensitivity position was about 0.95 or magnified x 100 equals to 95, increasing from the 1st sample to the 3rd sample. Furthermore, the standard deviation (σ) for the values of sensitivity position in the developed algorithm, has a value equals to $\sigma = 1.01$;
- **Edge threshold position:** as results appoints, the maximum value of edge threshold position were 0.94 or magnified x 100 equals to 94, where was a value increasing from the 6th sample to the 14th sample. While the lowest value of edge threshold position was about 0.20 in the 6th sample, magnified x 100 is equals to 20. Furthermore, the standard deviation (σ) for the values of edge threshold position in the developed algorithm, has a value equals to $\sigma = 25.29$;
- **Utilized method (phase code):** phase code is the name of the method utilized in the developed MATLAB R-2020 which refers to the threshold method for image binarization and segmentation;
- **Object polarity (bright):** the object polarity (bright) refers to the gray-scale tone adopted in the circular element detection using the developed algorithm. It means that the polarity of image is binarized to a value equals “1” in this image processing method;
- **Radius ranges (from 10 μ m to 30 μ m):** the radius range indicates the interval for the detected circles in the image processing algorithm. In other words, it means that the minimum radius of detected circles is equal “10 μ m” while the maximum value is about “30 μ m”;

The **Figure 19** shows the set of 14 eukaryotic protist cells images with circle detection. The dataset of those images can be founded in [20].

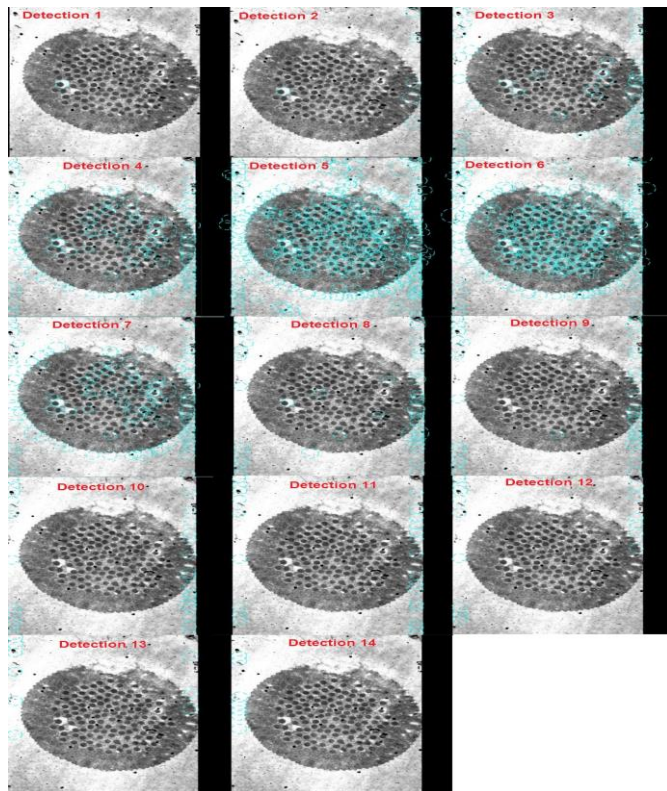


Figure 19. Set of 14 eukaryotic protist cells images with circle detection using MATLAB R2020 software

In the **Table 6** it's possible to observe the following measurements: number of detection; number of detected circles; sensitivity position values; edge threshold position; method; object polarity; and radius range, respectively. This table is composed by 7 columns and 15 lines.

Table 6. Measurement patterns utilized in this current research

Detection	Number of circles	Sensitivity Position	Edge Threshold Position	Method	Object Polarity	Radius Range
1	1	0.95	0.3	Phase Code	Bright	10 < R < 30
2	6	0.96	0.3	Phase Code	Bright	10 < R < 30
3	38	0.97	0.3	Phase Code	Bright	10 < R < 30
4	95	0.98	0.3	Phase Code	Bright	10 < R < 30
5	287	0.99	0.3	Phase Code	Bright	10 < R < 30
6	218	0.98	0.20	Phase Code	Bright	10 < R < 30
7	97	0.98	0.30	Phase Code	Bright	10 < R < 30
8	41	0.98	0.40	Phase Code	Bright	10 < R < 30
9	33	0.98	0.50	Phase Code	Bright	10 < R < 30
10	28	0.98	0.60	Phase Code	Bright	10 < R < 30
11	24	0.98	0.70	Phase Code	Bright	10 < R < 30
12	15	0.98	0.80	Phase Code	Bright	10 < R < 30
13	9	0.98	0.90	Phase Code	Bright	10 < R < 30
14	7	0.98	0.94	Phase Code	Bright	10 < R < 30

Thus, the maximum numbers of detected circles were 287, and the minimum number of detected circles was 1 detection, utilizing a threshold of 0.3. The table shown above expresses the measurement patters utilized in this current research. As the some metrics in the **Table 6**, such “method”, “objected polarity” and “radius range” are fixed in the MATLAB R2020 script, the pattern variables which are utilized to build the **Graphics**, are respectively: “detection”, “number of circles”, “sensitivity position” and “edge threshold position”.

Furthermore, the **Graphic 1** represents the number of circles by detection sample, as shows the **Figure 20**. It's possible to observe that the maximum number of detected circles were 287 (sample 5) and the minimum number of detected circles was 1 circle (sample 1).

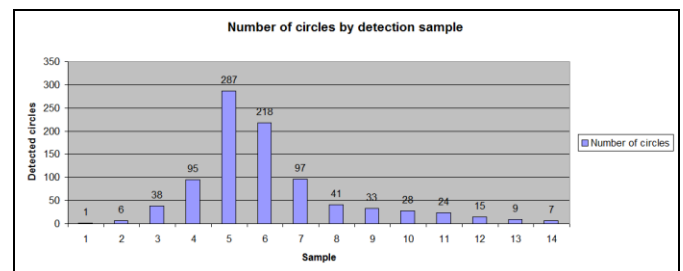


Figure 20. Graphic 1 – Number of circles by detection sample

Now, the **Graphic 2** shows the number of circles by sensitivity position (10² amplified). The **Figure 21** shows those correlations, and its possible to observe that after the 7th measurement, the sensitivity position was stabilized in 98, and the number of detected circles was beginning to decrease (from 41 detected circles – 8th measurement to 7 detected circles – 14th measurement).

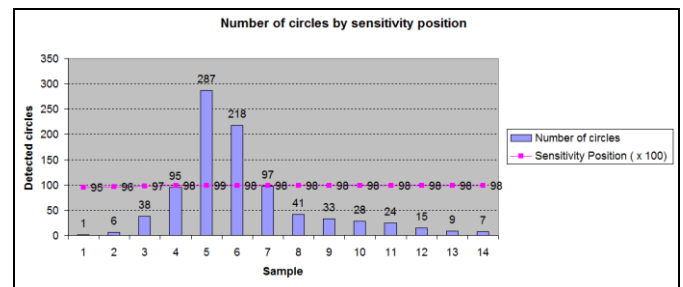


Figure 21. Graphic 2 – Number of circles by sensitivity position

Therefore, in the **Graphic 3**, it's observed the number of circles by edge threshold position (10² amplified). The **Figure 22** shows those correlations, and it's possible to observe that after the 6th measurement, the edge threshold position begins to growth (from 218 detected circles – 6th measurement to 7 detected circles – 14th measurement). Furthermore, this graphics shows that there was a growth about 370% in terms of edge threshold position increasing from the 6th measurement (edge threshold position: 0.20) to the 14th measurement (edge threshold position: 0.94). Now the number of detected circles decreases from 218 detected circles (6th measurement) to 7 detected circles (14th measurement) representing a percentage difference about 96.78%.

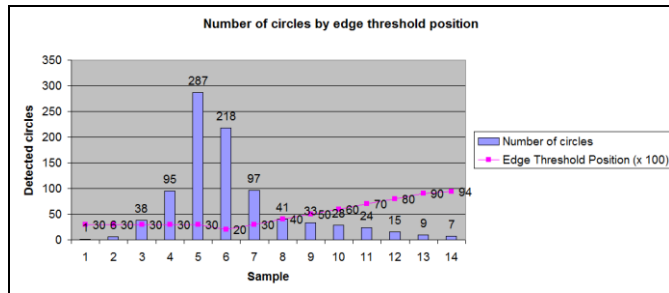


Figure 22. Graphic 3 – Number of circles by edge threshold position

Looking now to the **Graphic 4** represented by the **Figure 23**, its possible to observe the correlation of percentage difference for those utilized patterns: detected circles difference (minimum 1; maximum 287 – percentage difference of 28,600%); sensitivity position difference (minimum 0.95 in the 1st sample; maximum 0.98 – percentage difference of 3.15%); edge threshold position difference (minimum 0.20; maximum 0.94 – percentage difference of 370%).

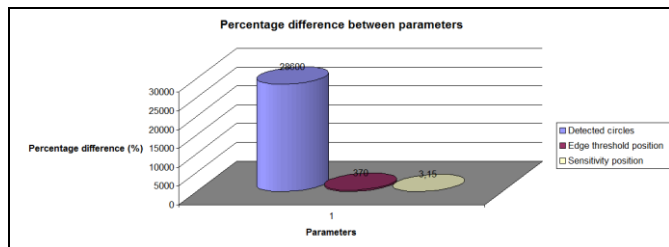


Figure 23. Graphic 4 – Percentage difference between parameters

Furthermore, the **Graphic 5** appoints to the moving average for the number of circles of detection samples. In the **Figure 24**, it's possible to observe that the peak of this average is concentrated on the 6th sample, where the number of detected circles is equals to 218 elements, for example. Thus, in concern to the standard deviation (σ) to the parameters, such as: sensitivity position; edge threshold position and number of detected circles. The obtained results were values of: $\sigma = 1.01$ (sensitivity position); $\sigma = 25.29$ (edge threshold position); and $\sigma = 86.19$ (number of detected circles). In addition, those results indicates that there was a estimative of the standard deviation based on the 14 analyzed eukaryotic cells samples that has been runned in the MATLAB algorithm. It means that the standard deviation is a measure of how widely values are dispersed from the mean value, or the respective average. Thus, the **Graphic 6** in the **Figure 25** shows the values cited above for the selected algorithm parameters. Is also represented below the formula of standard deviation in Eq.(4):

$$\sigma = \sqrt{\frac{\sum(x - \bar{x})^2}{(n - 1)}} \tag{4}$$

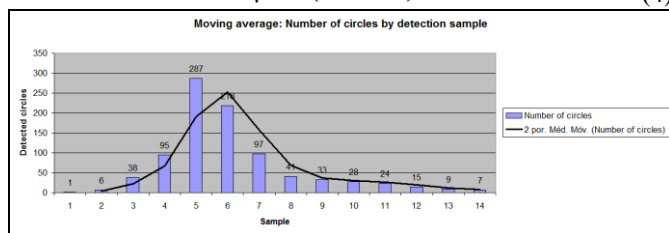


Figure 24. Graphic 5 – Moving average for the number of circles by detection sample

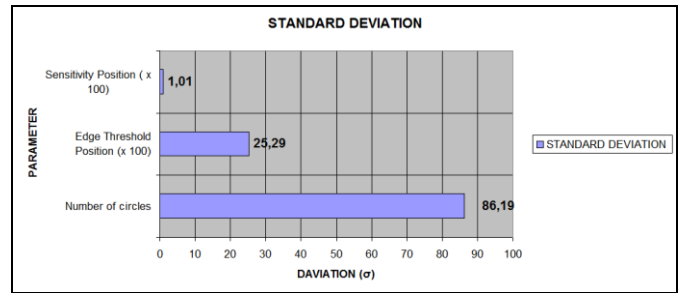


Figure 25. Graphic 5 – Standard deviation (σ) for the selected algorithm parameters

Comparing in the context of other work reported in the literature [9], this current research have been obtained a graphical algorithm interface in MATLAB R2020 more intuitive and easily to detect circular elements in the set images of 14 eukaryotic protist cells, as shows the **Figure 26** below:

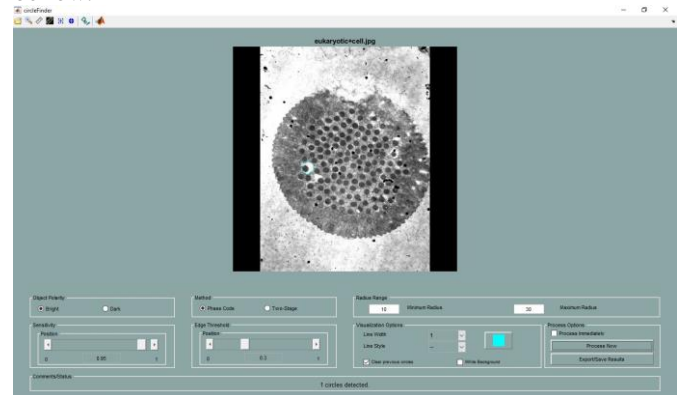


Figure 26. Graphical algorithm interface in MATLAB R2020

Therefore, as discussion, this experiment has obtained a better detection of circular elements in eukaryotic protist cells when the sensitivity position is setting at 0.99 and the edge threshold position is about 0.3: within phase code method, bright object polarity and radius range between 10 μ m and 30 μ m. These values were obtained using MATLAB-R2020. Once again as a discussion topic, the accuracy of the proposed algorithm, have shown better when the parameters such as sensitivity position presents the value about 0.95 to 0.97 and the named pattern edge threshold position has the values about 0.20 to 0.30, as can see in the graphics presented in this section. Furthermore, as a important discussion topic is in concern to the moving average and standard deviation: according to the **Graphic 5**, the peak of moving average it's about 218 detected circles, and as a standard deviation, the value is about $\sigma = 86.19$, indicating that this conjunction measurement are scattered, once the value of detected circles for those 14 samples are very heterogeneous.

Discussion and future research

Still, as taken future research and limitations into account this work, as proposed future works its profitable that MATLAB R2020 circle detection algorithm can be capable to interact with any kind of cells, such as: heart cells, stomach cells, skin cells, brain cells, among other kind of eukaryotic cells. Furthermore, as a future scope, would be proposed a specific embedded hardware utilizing an enhanced algorithm to

support the medical image analysis procedures, and return great results when cells images taken by a microscope need to be analyzed for healthcare professionals. In terms of discussion, the **Figure 26** indicates the state of the art about the MATLAB algorithm detection circles screens. Looking at this figure, it's possible observe that algorithm patterns, such as: number of detected circles; sensitivity position; edge threshold position; method; object polarity; radius range; and line thickness; are very easily to modify the entry values, and new measurements can be taken from this features contained in the developed MATLAB algorithm.

10. Conclusion and Future Scope

This research has proven to be a contribution to the field of biomedicine and biotechnology in terms of techniques for analysis and identification of eukaryotic protist cells using the Epsom Perfection V750 Microscope.

Thus, according to the parameters established by the detection algorithm, such as: sample number (from 1 to 14); number of circles detected; sensitivity position; edge threshold position; method; object polarity; radius range; it was possible to draw objective results and conclusions regarding the efficiency of the algorithm in MATLAB and its applicability in biomedical parameters, for example.

Therefore, as results we obtained the rate of the number of circles detected per sample, where sample number 5 proved to have the highest concentration of detected elements, with 287 observable circles; it was also proposed to measure the position of sensitivity of the algorithm according to the sample number, where the results indicated a stability of 0.98 from the 7th sample to the 14th sample, for a cell radius of 10µm to 30µm; the number of circles per edge threshold position was also compared, where the percentage difference between the 6th sample and the 14th sample was approximately 96.78%.

As for the limitations of this work, they refer to the possibility of having it adapted to an embedded hardware, where it could analyze in real time the number of circles composed in a mass test of eukaryotic cell analysis. Therefore, this does not take away the relevance of this project, which can open opportunities for other researchers to find a cheap and effective method to accurately analyze cell content.

Now as an application and recommendation, it is recommended that this scientific research be used in cell analysis laboratories so that a large amount of circular elements in cells can be analyzed. With the algorithm developed, this work proved to be highly efficient, with a total number of 287 elements detected in protist eukaryotic cells, position sensitivity of 0.99, maximum edge threshold position values of 0.94 and established standards such as: phase code method; bright object polarity; and radius range about 10µm to 30µm. Above all, as future works, it is possible that, in addition to developing an embedded version of the algorithm, it can also detect elements in cells of

different organs of the human body, such as: heart, stomach, brain, muscle tissue and lungs.

Data Availability

Readers can access the data supporting the conclusions of the study through ISROSET website (<https://www.isroset.org/index.php>). Thus, unavailable data cannot be released until the ISROSET article releasing. Study Limitations: none.

Conflict of Interest

The authors declare that they do not have any conflict of interest.

Funding Source

Funding source: none.

Authors' Contributions

Author-1: researched literature and introduction of the study. Author-2: algorithm validation method. Author-3: reviewing the remaining topics.

Acknowledgements

The authors of this current manuscript acknowledgement the Laboratory of Visual Communications (LCV) for all the granted support in the laboratory activities to the development of this research. The (LCV) also is acknowledged for all the resource and support given in the all steps of this research.

References

- [1]. SBEB (Sociedade Brasileira de Engenharia Biomédica). "Engenharia Biomédica: o elo entre engenharia, ciências da saúde e sociedade". Rio de Janeiro – Brazil, 2017, pp.01-03, 2017.
- [2]. LAM, W. "Perspectivas da biotecnologia em 2022: Após um ano difícil, a biotecnologia tem o potencial de despertar em 2022," *Franklin Equity Group*. São Paulo – Brazil, pp.03-06, 2021.
- [3]. BIOPHARMA TREND. "AI Drug Discovery: Key Trends and Developments in Pharmaceutical Industry". Brentford – England, pp.05-07, 2023.
- [4]. MORDOR INTELLIGENCE. "Mercado de descoberta de medicamentos – crescimento, tendências, impactos do COVID-19 e previsões (2023 – 2028)". Telangana – Índia, pp.01-06, 2023.
- [5]. QIAO, L. et. al. "A circuit for secretion-coupled cellular autonomy in multicellular eukaryotic cells," *Molecular Systems Biology*, Vol. 19, Issue 12, pp.1-27, 2023.
- [6]. BARREIRO, E.J. et. al. "Biodiversidade: fonte potencial para a descoberta de fármacos," *Quim. Nova*, Vol. 32, No. 3, pp.679-688, 2009.
- [7]. BHAVANI, M. et. al. "Streamlined Classification of Microscopic Blood Cell Images," *International Journal of Intelligent Systems and Applications in Engineering*, Vol. 11, No. 1, pp. 57-62, 2023.
- [8]. MATSUURA, K. et. al. "Blood Cell Separation Using Polypropylene-Based Microfluidic Devices Based on Deterministic Lateral Displacement," *Micromachines*, Vol. 14, No. 238, pp.1-13, 2023.
- [9]. MERZOUG, A. et. al. "Lesions Detection of Multiple Sclerosis in 3D Brian MR Images by Using Artificial Immune Systems," *International Journal of Cognitive Informatics and Natural Intelligence and Support Vector Machines*, Vol. 15, No. 2, pp.1-14, 2021.
- [10]. SARKAR, C. et. al. "Artificial Intelligence and Machine Learning Technology Driven Modern Drug Discovery and Development," *International Journal of Molecular Sciences*, Vol.

24, No. 2026, pp.1-40, 2023.

- [11]. SOUDAH, T. et. al. "Desorption electrospray ionization mass spectrometry imaging in discovery and development of novel therapeutics," *WILEY – Mass Spec*, Vol. 42, No. 1, pp.751-778, 2021.
- [12]. RASHID, P.Q. "Sars COV-2 CT-Scan Image Classification Using Graph Convolutional Networks," *International Istanbul Modern Scientific Research Congress – IV*, pp.160-165, 2022.
- [13]. HASAN, M. et. al. "Review on the Evaluation and Development of Artificial Intelligence for COVID-19 Containment," *MDPI Sensors*, Vol. 23, No. 527, pp.1-35, 2023.
- [14]. MIRSHAFIEI, M. et. al. "Application of MIA-QSAR in Designing New Protein P38 MAP Kinase Compounds Using a Genetic Algorithm," *Periodica Polytechnica Chemical Engineering*, Vol. 67, No. 1, pp.141-160, 2023.
- [15]. LOPES, S. "Bio: volume único – 1. ed.," *Saraiva*. São Paulo – Brazil, pp.38-126, 2004.
- [16]. IANO, Y. et. al. "Analysis of Results of Some Techniques for the Recognition of Circular Shapes in the Steel Bar Counting System Using Image Processing," *Proceedings of the 6th Brazilian Technology Symposium (BTSym'20)*, Vol. 6, No. 1, pp.1-11, 2021.
- [17]. HART, P.E. et. al. "How the Hough transform was invented [DSP History]," *IEEE Signal Process. Mag*, Vol. 26, No. 1, pp. 18–22, 2009.
- [18]. SHAPIRO, L. et. al. "Computer Vision," *Prentice Hall*. United States, pp.608-615, 2001.
- [19]. X. CHEN, L. LU, AND Y. GAO, "A new concentric circle detection method based on Hough transform," *ICCSE 2012 - Proc. 2012 7th Int. Conf. Comput. Sci. Educ.*, no. Iccse, pp. 753–758, 2012.
- [20]. CELL IMAGE LIBRARY. "CIL Image Viewer – Open source," *UCSD*. United States, pp.01-14, 2023.
- [21]. P. SHARNAGAT, K.P. JAISWAL. "Assessment of Enteropathogens from Fresh Vegetables Associated Serious Risks to Human Health," *International Journal of Scientific Research in Biological Sciences*, Vol. 10, No. 1, pp.12-17, 2023.
- [22]. FERRARI, I.V. et. al. "Molecular Docking studies against Glioblastoma Proteins," *International Journal of Scientific Research in Biological Sciences*, Vol. 10, No. 2, pp.19-23, 2023.

AUTHORS PROFILE

Daniel Katz Bonello, MSc. Graduate in Control and Automation Engineering at Universidade Paulista – UNIP (2016), Campinas-Brazil, also holds a MSc degree in Electrical Engineering (2020) at UNICAMP. Research Interests: Computer Vision, Image Processing, Machine Learning, Automation Strategies.



Yuzo Iano, PhD. Prof. Yuzo Iano is the head and founder of the Laboratory of Visual Communications since 1972. He obtained his BSc (1972), MSc (1974) and PhD (1986) in Electrical Engineering at UNICAMP, SP-Brazil. Research Interests: Digital Signal Processing, Pattern Recognition, Internet of Things, Digital TV.



Umberto Bonello Neto, MSc. Graduate in Building Technology at UNICAMP, SP-Brazil (1987), also holds a MSc degree in Electrical Engineering (2021) at UNICAMP. Research Interests: Process Control Strategies, Fieldbus Technology, Deep Learning, PCB design.



Int. J. of Scientific Research in
Biological Sciences

www.isroset.org

Int. J. of Scientific Research in
Chemical Sciences

www.isroset.org

Int. J. of Scientific Research in
**Computer Science and
Engineering**

www.isroset.org

World Academics Journal of
Engineering Sciences

ISSN: 2348-635X

www.isroset.org

Journal of
Physics and Chemistry of Materials

ISSN: 2348-6341

www.isroset.org

ISSN: 2349-3178 (Print),
ISSN: 2349-3186 (Online)

**International Journal of
Medical Science
Research and Practice**

Published by ISROSET



Submit your manuscripts at
www.isroset.org
email: support@isroset.org

[Make a Submission](#)

Int. J. of Scientific Research in
**Mathematical and
Statistical Sciences**

www.isroset.org

Int. J. of Scientific Research in
**Multidisciplinary
Studies**

www.isroset.org

Int. J. of Scientific Research in
**Network Security
and Communication**

e-ISSN: 2321-3256

World Academics Journal of
Management

ISSN: 2321-905X

www.isroset.org

Int. J. of Scientific Research in
**Physics and
Applied Sciences**

www.isroset.org

Int. J. of Computer
Sciences and Engineering

www.ijcseonline.org

Call for Papers:

Authors are cordially invited to submit their original research papers, based on theoretical or experimental works for publication in the journal.

All submissions:

- must be **original**
- must be **previously unpublished research results**
- must be **experimental or theoretical**
- must be in **the journal's prescribed Word template**
- and will be **peer-reviewed**
- may not be **considered for publication elsewhere at any time during the review period**

[Make a Submission](#)